Modification of the Gravity Wave Parameterization in the Whole Atmosphere Community Climate Model: Motivation and Results

ROLANDO R. GARCIA, ANNE K. SMITH, DOUGLAS E. KINNISON, AND ÁLVARO DE LA CÁMARA

National Center for Atmospheric Research,[a] *Boulder, Colorado*

DAMIAN J. MURPHY

Australian Antarctic Division, Hobart, Tasmania, Australia

(Manuscript received 4 April 2016, in final form 13 October 2016)

ABSTRACT

The current standard version of the Whole Atmosphere Community Climate Model (WACCM) simulates Southern Hemisphere winter and spring temperatures that are too cold compared with observations. This ''cold-pole bias'' leads to unrealistically low ozone column amounts in Antarctic spring. Here, the cold-pole problem is addressed by introducing additional mechanical forcing of the circulation via parameterized gravity waves. Insofar as observational guidance is ambiguous regarding the gravity waves that might be important in the Southern Hemisphere stratosphere, the impact of increasing the forcing by orographic gravity waves was investigated. This reduces the strength of the Antarctic polar vortex in WACCM, bringing it into closer agreement with observations, and accelerates the Brewer–Dobson circulation in the polar stratosphere, which warms the polar cap and improves substantially the simulation of Antarctic temperature. These improvements are achieved without degrading the performance of the model in the Northern Hemisphere stratosphere or in the mesosphere and lower thermosphere of either hemisphere. It is shown, finally, that other approaches that enhance gravity wave forcing can also reduce the cold-pole bias such that careful examination of observational evidence and model performance will be required to establish which gravity wave sources are dominant in the real atmosphere. This is especially important because a ''downward control'' analysis of these results suggests that the improvement of the cold-pole bias itself is not very sensitive to the details of how gravity wave drag is altered.

1. Introduction

In coupled integrations of the Whole Atmosphere Community Climate Model (WACCM), feedbacks among chemistry, radiation, and dynamics control the model climatology. Changes to any of these components of the model can produce changes, often undesirable, in other aspects of the simulated climate. Solomon et al. (2015) have described improvements to the heterogeneous chemistry parameterization used in WACCM motivated by the work of Wegner et al. (2013). When the new chemical scheme is used in fully coupled integrations, important biases develop in the simulation of Antarctic ozone. Specifically, simulations that incorporate the new heterogeneous chemistry scheme tend to produce unrealistically large ozone loss over Antarctica. The proximate cause of the low-ozone problem in WACCM is the model's ''cold-pole bias'' in the Antarctic stratosphere: that is, the fact that it calculates polar temperatures considerably colder than observed during Antarctic winter and spring. In the new chemistry scheme, heterogeneous processing of halogen compounds (and hence ozone loss) responds sensitively to temperature; as a result, accurate simulation of temperature in the lower polar stratosphere becomes crucial for calculating ozone loss correctly. Furthermore, the cold-pole bias is amplified because low ozone in Antarctic spring leads to weaker solar heating, which in turn results in further cooling.

Although the feedback between temperature and ozone compounds the cold-pole problem, both temperature and ozone biases in WACCM ultimately arise

[a] The National Center for Atmospheric Research is sponsored by the National Science Foundation.

Corresponding author e-mail: Rolando R. Garcia, rgarcia@ucar.edu

DOI: 10.1175/JAS-D-16-0104.1

from deficiencies in the model's dynamics. Temperature in the polar stratosphere is strongly influenced by the downwelling branch of the wave-driven Brewer–Dobson circulation (BDC), which produces adiabatic warming. This implies that wave forcing of the BDC in WACCM is too weak in Southern Hemisphere winter. The extratropical BDC is forced by planetary waves and gravity waves. Forcing due to planetary waves is determined by wave generation, propagation, and dissipation consistent with the resolved dynamics and cannot be modified ad hoc. On the other hand, gravity waves are parameterized because they cannot be simulated explicitly at the moderate spatial and temporal resolution (~2° and 0.5 h, respectively) that, for practical reasons, must be used in a climate model such as WACCM. Parameterizations of three different sources of gravity waves are included in WACCM: stationary waves generated by flow over orography (McFarlane 1987), waves with a spectrum of phase speeds generated by convection (Beres et al. 2005), and waves with a spectrum of phase speeds generated by fronts (Richter et al. 2010). All three formulations include parameters that can be adjusted within reasonable limits to improve the overall performance of the model.

Some current work points to the importance of gravity waves forced by orography in the momentum budget of the Southern Hemisphere. For example, McLandress et al. (2012) noted that most chemistry–climate models exhibit systematic zonal-mean temperature and zonal wind biases in the Southern Hemisphere and that these biases could be related to a deficit of orographic gravity wave drag near 60°S. They also demonstrated that the dynamical climatology of the Canadian Middle Atmosphere Model above Antarctica improved considerably when an additional source of orographic gravity waves centered on 60°S was prescribed. Alexander and Grimsdell (2013) argued that the deficit of gravity wave activity at 60°S might be related to mountainous island sources in the Southern Ocean, which are not properly resolved in the models. Sato et al. (2012) concluded from the results of very-high-resolution numerical simulations that orographic gravity waves can propagate horizontally into oceanic regions from remote mountain sources. Hindley et al. (2015) used global positioning system data to confirm that wave activity near 60°S propagates from lower latitudes over the Southern Andes. On the other hand, Hendricks et al. (2014) and Shibuya et al. (2015) have argued that a substantial fraction of gravity wave activity over the Southern Ocean appears to be associated with nonorographic sources, such as storms tracks in the troposphere; and several observational studies have documented large, intermittent momentum fluxes over the Southern Ocean (Hertzog et al. 2012; Wright et al. 2013; Alexander 2015; Jewtoukoff et al. 2015). Following these observations, De la Cámara et al. (2016) have recently shown that accounting for large, sporadic momentum fluxes in the nonorographic gravity wave parameterization improves the simulation of the final warming in the Antarctic stratosphere in a general circulation model.

A close examination of how the orographic gravity wave parameterization is implemented in WACCM reveals that it is likely to underestimate the forcing in the Southern Hemisphere. In the orographic parameterization [see McFarlane (1987) for details], the amplitude of waves forced by flow over topography is a function of the standard deviation σ of the subgrid-scale topography, which is computed from the variance of a high-resolution-topography dataset about the smooth topography resolved by the model grid. When sharp topographic features are located near oceans, σ can be nonzero in grid cells that are located entirely over water. To deal with this perceived problem, the wave drag produced by the orographic parameterization in WACCM is multiplied by a high-resolution "land fraction" factor F_L, which is equal to the fraction of the grid cell that contains land. This eliminates drag over ocean grid cells but also has the effect of reducing it in grid cells that contain sharp topographic features and border on, or are surrounded by, oceans. In the Northern Hemisphere, many of the main topographic features (e.g., the U.S. Rocky Mountains, the Alps, the Himalayas, and the Tibetan Plateau) are not immediately adjacent to oceans, so the use of F_L has a relatively minor impact on the parameterized gravity wave drag. In the Southern Hemisphere, on the other hand, the principal topographic barriers (e.g., the Andes, the Palmer Peninsula, and various mountainous islands in the Southern Ocean) are located within a grid cell of, or completely surrounded by, oceanic regions. In these instances, the use of F_L has a substantial impact on orographic gravity wave forcing. Regardless of the merits of using F_L to suppress orographic forcing over oceanic grid cells, it is clear that this procedure reduces selectively orographic wave drag in the Southern Hemisphere relative to the Northern Hemisphere.

Another peculiarity of the orographic gravity wave parameterization currently used in WACCM is that the magnitude of the wave fluxes is estimated without taking into account the orientation of the low-level wind with respect to topographic barriers (McFarlane 1987). In the Southern Hemisphere, especially at high latitudes, the main topographic barriers (the Andes, the Palmer Peninsula, and the Southern Alps of New Zealand) are oriented mainly north–south, and therefore approximately normal to the direction of the prevailing, strongly zonal westerly flow. In the Northern Hemisphere, the

tropospheric flow is much less zonal, and the topography itself does not have a predominant north–south orientation everywhere. As a result, the failure to account for the orientation of background flow with respect to topography will tend to underestimate orographic gravity wave fluxes in the Southern Hemisphere relative to the Northern Hemisphere.

The purpose of this study is to describe how the parameterization of gravity waves in WACCM might be modified to account for the deficiencies described above and to demonstrate the impact of such modifications on the simulation of the Antarctic ozone hole and on the dynamics and temperature of the middle atmosphere in both hemispheres. The current version of WACCM, with updated stratospheric chemistry, is described in section 2, where the impact of changes in the representation of heterogeneous chemical processes is also discussed. In section 3, we outline the modifications made to the orographic gravity wave parameterization and discuss their impact on the model's chemistry and dynamical climatology. We emphasize changes in temperature and ozone in the Antarctic stratosphere, but we also document the behavior of other important features of the model, including the temperature structure of the polar mesosphere and the climatology of stratospheric temperature and sudden warmings in the Northern Hemisphere, which are essential measures of performance for a ''high top'' model such as WACCM. In section 4, we illustrate the changes in wave forcing that result from modification of the gravity wave parameterization and present a downward control analysis of changes in polar downwelling in the Southern Hemisphere due to enhanced orographic gravity wave drag. We show that, consistent with recent studies (McLandress et al. 2012; Cohen et al. 2013, 2014; Sigmond and Shepherd 2014), changes in gravity wave drag are accompanied by changes in the Eliassen–Palm (EP) flux divergence of resolved waves such that substantial ''compensation'' occurs between the two. While the focus of this study is on the orographic gravity wave parameterization, changes to the parameterization of waves excited by fronts can also improve the model's cold-pole bias, and we address this point in section 5. Section 6 summarizes our findings and discusses the uncertainties associated with modifying gravity wave parameterizations to improve the dynamical performance of models such as WACCM.

2. The Whole Atmosphere Community Climate Model

WACCM is a high-top model that can be used as the atmospheric component of the Community Earth System Model (CESM1) of the National Center for Atmospheric Research. The version used in this study, WACCM4, is based on the Community Atmosphere Model, version 4 (CAM4; Neale et al. 2013). The horizontal resolution is 2.5° × 1.9° (longitude × latitude); vertical resolution varies with altitude, from 1.1 to 1.4 km in the troposphere (above the boundary layer) and lower stratosphere to 1.75 km in the upper stratosphere and 3.5 km in the upper mesosphere and lower thermosphere. The upper boundary is located at a geometric altitude of about 140 km. The external forcings, such as anthropogenic gas emissions, volcanic aerosols, and solar flux, vary more or less smoothly with calendar day and year based on observations or—in the case of the solar flux—on an empirical model. On the other hand, day-to-day and interannual behavior is strongly affected by the model's intrinsic dynamical variability. Such a free-running model is necessary to evaluate interactions and feedbacks in the coupled chemistry–climate system. Marsh et al. (2013a) describe the model features and present results from simulations made for the fifth phase of the Coupled Model Intercomparison Project (CMIP5).

WACCM may also be run in ''specified dynamics'' mode (SD-WACCM). In SD-WACCM, temperature and horizontal winds in the troposphere and stratosphere, as well as surface fluxes, are relaxed every time step toward data from NASA's Modern-Era Retrospective Analysis for Research and Applications (MERRA; Rienecker et al. 2011; Lamarque et al. 2012) such that the calculated dynamical and temperature fields up to about 50 km follow closely the reanalysis. The procedure used to constrain the model is described by Marsh (2011) and Kunz et al. (2011). We emphasize that chemical composition is not directly constrained but is determined jointly by the constraints on temperature and dynamics and the model's photochemical scheme. By constraining dynamical variability to reanalysis data, SD-WACCM is useful for evaluating model chemistry by direct comparison to chemical observations in the stratosphere.

The chemical mechanism used in WACCM4 is based on that described by Kinnison et al. (2007) and used in the CMIP simulations of Marsh et al. (2013a), except that a new, more realistic parameterization of heterogeneous chemical processes has been implemented, as described next.

a. *Updated heterogeneous chemistry*

Heterogeneous chemical processes are central to the formation of the Antarctic ozone hole. The parameterization of these processes has been updated by Solomon et al. (2015) following the work of Wegner et al. (2013),

who introduced major improvements in the simulation of denitrification and of the seasonal evolution of HNO_3, H_2O, and polar stratospheric clouds in the specified dynamics version of WACCM. Specifically, the representation of the uptake of HNO_3 in the formation of nitric acid trihydrate and supercooled ternary solutions was modified, as was the threshold for the supersaturation of water to form ice. This produces excellent agreement in the relationship between temperature-dependent removal of gas-phase HNO_3 compared to *Aura* MLS satellite observations (cf. Wegner et al. 2013, their Fig. 2). Because the new heterogeneous chemistry parameterization alters the simulation of polar stratospheric cloud composition and occurrence, it also affects the heterogeneous reactions that activate chlorine and bromine and produce the ozone hole.

b. *The impact of updated chemistry*

Figure 1 compares September-average ozone column derived from ozonesonde observations at Halley Bay (75°S, 26°W) with results from two WACCM simulations. The first of these, labeled REF and denoted by the red crosses, is a reference, free-running simulation with fully coupled chemistry that includes the updated heterogeneous chemistry described above but no other changes to the model. We note, however, that REF and other free-running simulations discussed in this paper use specified sea surface temperatures (SST) from the Hadley Centre Sea Ice and Sea Surface Temperature dataset (HadISST; Rayner et al. 2003) to make them directly comparable to a simulation with specified dynamics, introduced below, wherein SST are prescribed from the same source. Nevertheless, we have verified that the improvements in the simulation of Antarctic polar cap temperatures and ozone described later are also present in WACCM simulations with a fully coupled ocean.

In simulation REF the ozone column is underestimated substantially, by up to 25%–30% in the late 1990s, compared to the Halley measurements (black squares in Fig. 1). On the other hand, a specified dynamics simulation (REF-SD-MERRA; blue triangles) follows closely the observed behavior. In REF-SD-MERRA all dynamical fields and the temperature field in the stratosphere are constrained by MERRA data. Part of the excellent agreement is due to the fact that the influence of dynamic variability is largely removed in specified dynamics simulations; however, the elimination of the systematic low bias in ozone column amounts seen in the free-running simulation, REF, is due principally to the absence of a cold-pole bias in REF-SD-MERRA.

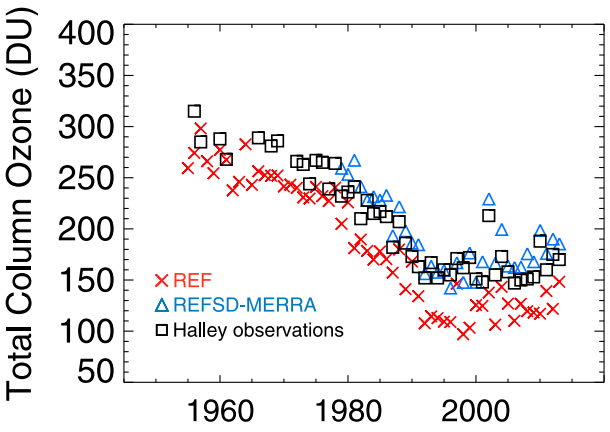

FIG. 1. September monthly mean ozone column (DU) at Halley Bay (75°S, 26°W) in two WACCM simulations compared to the column derived from ozonesonde observations (black squares). REF (red crosses) is a standard WACCM simulation with no changes to the GW parameterization; REF-SD-MERRA (blue triangles) is a simulation constrained by MERRA data in the stratosphere.

The cold-pole bias in the standard, free-running version of WACCM is large. Figure 2 shows a comparison of Antarctic zonal-mean temperature averaged over the polar cap (60°–90°S) in the REF simulation versus MERRA data. This comparison, as well as others discussed below, is based on daily climatological averages for the period 1980–2010, which is covered by MERRA. Figure 2a shows the MERRA climatology, and Fig. 2b shows the difference between simulation REF and MERRA. Stippled areas in this and similar comparisons denote differences that are statistically insignificant at the 95% confidence level according to a Student's t test. The cold bias in the critical altitude range of 12–24 km, where heterogeneous activation of halogen compounds leads to the formation of the ozone hole, ranges from about −5 to −15 K. The largest bias, seen during the transition period from late spring to summer (late November–January), is associated with the delayed breakdown of the polar vortex in the lower stratosphere in simulation REF and is not directly relevant to the simulation of ozone loss. While the cold bias in September and October, the period that is most important for ozone chemistry, is smaller (−5 to −10 K), it still leads to unrealistically large ozone loss, as seen in Fig. 1. Figure 3a shows the seasonal cycle of daily polar cap temperature at 85 hPa (~17 km), in the core of the Antarctic ozone hole region, in REF (black solid curve) and MERRA (black dashed curve); the difference between the two is shown in Fig. 3b (black curve). The low temperature bias at 85 hPa is statistically significant throughout the year; during winter it averages −3 to −4 K, but becomes

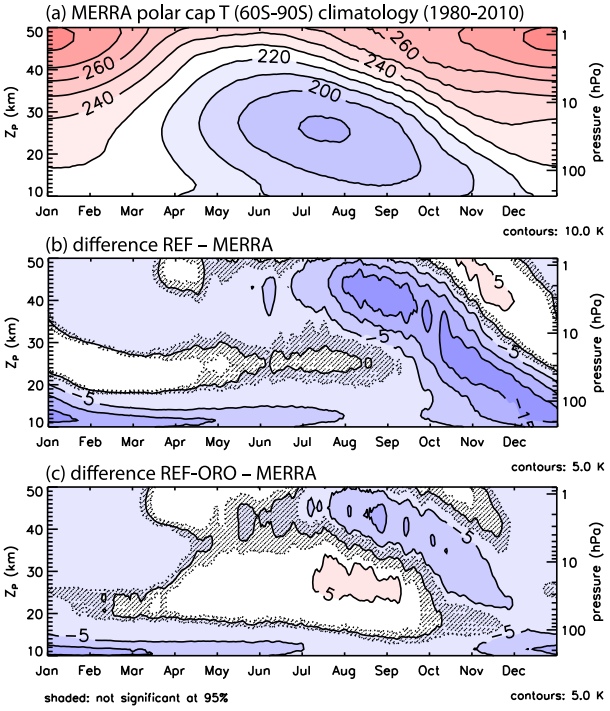

FIG. 2. (a) Climatological seasonal cycle of Antarctic polar cap temperature (K) from MERRA daily data; (b) difference between REF and MERRA; and (c) difference between REF-ORO and MERRA. Stippling denotes differences statistically insignificant at the 95% confidence level. Contour intervals are 10 K in (a) and 5 K in (b) and (c).

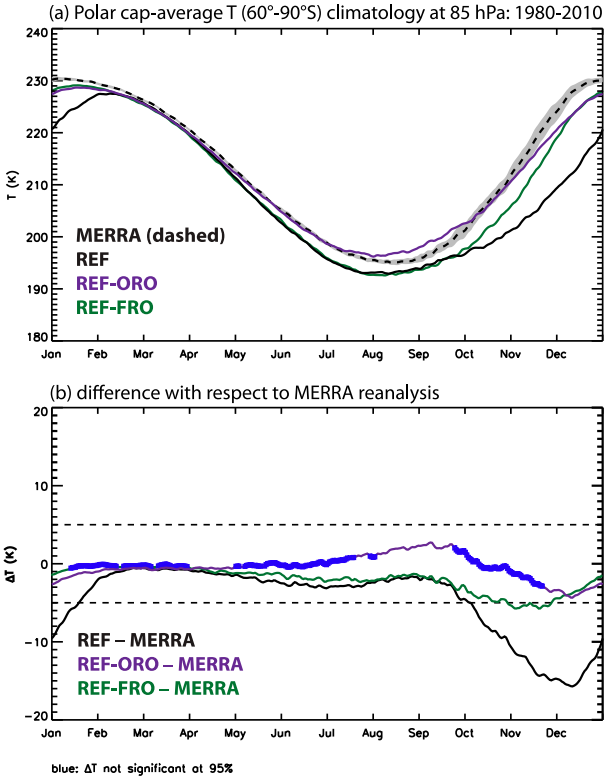

FIG. 3. (a) Climatological seasonal cycle of daily temperature (K) in the southern polar cap at 85 hPa from MERRA (shading denotes 2σ errors), REF, REF-ORO, and REF-FRO. (b) Differences between each simulation and MERRA. In (b), the dashed lines denote differences of ± 5 K; the blue shading denotes differences that are insignificant at the 95% level.

much larger in spring, when rapid ozone destruction occurs; it exceeds -5 K by late September and -10 K by late October.

3. Modification and validation of the gravity wave parameterization

a. Formulation

As noted in the introduction, the main topographic barriers in the Southern Hemisphere (the Andes, the Palmer Peninsula, and the Southern Alps of New Zealand) are oriented mainly north–south and therefore approximately normal to the direction of the strong zonal westerly flow, whereas this is not generally true of the Northern Hemisphere. The orographic gravity wave parameterization currently used in WACCM ignores this difference and prescribes a source stress for orographic gravity waves that is based only upon the standard deviation of the subgrid-scale topography (without reference to its orientation) and the magnitude of the wind at the source level. This tends to underestimate the flux of orographic gravity waves in the Southern Hemisphere relative to the Northern Hemisphere.

We test the role of enhanced orographic gravity wave forcing in the Southern Hemisphere by the simple expedient of doubling the magnitude of the orographic source flux everywhere in the Southern Hemisphere. Ideally, this would be accomplished by using a parameterization that accounts explicitly for the orientation of airflow over local topography. While such parameterizations exist (e.g., Scinocca and McFarlane 2000), they have not been implemented in any version of WACCM to date. Therefore, the simulation discussed here, with doubled orographic fluxes in the Southern Hemisphere only, constitutes an assessment of the sensitivity of WACCM to enhanced forcing by orographic gravity waves in that hemisphere. In addition, we have removed everywhere the land fraction factor F_L discussed in the introduction. The effect of F_L is most important in the Southern Hemisphere, where the main topographic features are adjacent to oceans. We illustrate and quantify the impact of F_L in section 5.

In the comparisons that follow, we refer to the simulation that uses the modified orographic gravity wave parameterization as REF-ORO, with the understanding

that it also includes the updated heterogeneous chemistry discussed in section 2a. We consider in turn the effects on the Southern Hemisphere stratosphere, the polar mesosphere and, finally, the stratosphere of the Northern Hemisphere.

b. *The Southern Hemisphere stratosphere: Temperature, zonal wind, and ozone*

The modification of the orographic gravity wave source stress has a notable impact on the temperature and zonal wind climatologies in the Southern Hemisphere. Figure 2c shows the difference in the seasonal cycle of polar cap temperature between REF-ORO and MERRA. While significant differences remain, much of the systematic cold bias has been removed (cf. Figs. 2b and 2c); in fact, from about mid-September through mid-November the new simulation is statistically undistinguishable from MERRA in the altitude range 15–20 km, near the core of the ozone-depletion region over Antarctica.[1] The major remaining discrepancies are a slight warm bias at 25–30 km in August and September and a remaining cold bias that descends from the upper to the lower stratosphere in Antarctic spring and early summer (September–December). The latter is a reflection of the fact that, despite the overall improvement of the temperature climatology, the breakdown of the southern polar vortex in the stratosphere still lags the climatological behavior. This may be seen in Fig. 4, which compares the seasonal cycle of the zonal-mean zonal wind $\overline{U}$ at subpolar latitudes (55°–65°S) in REF-ORO and MERRA. Above about 30 km, $\overline{U}$ is stronger in midwinter (June–July) by as much as 25 m s^{-1} in REF-ORO compared to MERRA; however, below that altitude the differences are generally smaller than 5 m s^{-1}, except in late spring and early summer (November–December), when $\overline{U}$ in REF-ORO is stronger than MERRA by over 10 m s^{-1}. Note also that the reversal of $\overline{U}$, from westerly to easterly, occurs in MERRA in late November but is delayed in REF-ORO until mid-December. While the discrepancies between REF-ORO and MERRA are not small during the transition from Austral spring to summer, they are much reduced compared to the REF simulation, in which the zero-wind line never reaches the 10-hPa level and the differences from the MERRA climatology at other times of the year are generally over twice as large as those seen in Fig. 4 (not shown).

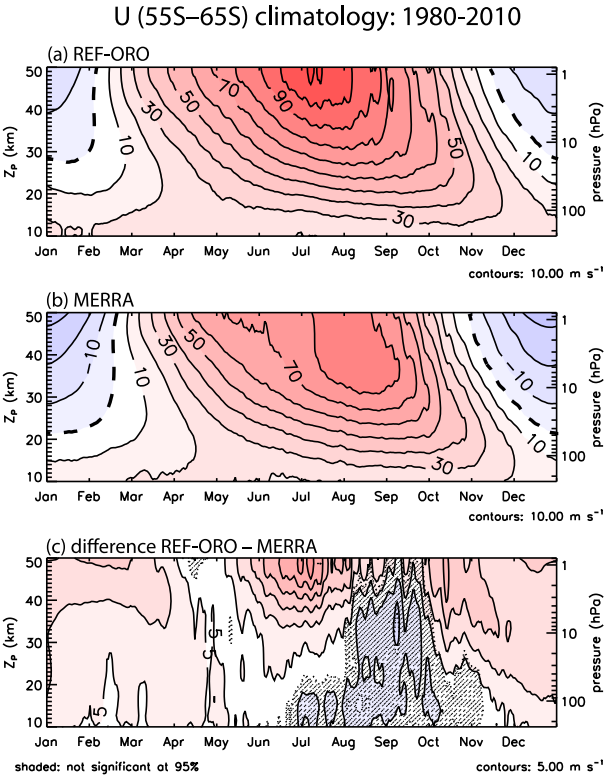

FIG. 4. Seasonal cycle of daily zonal-mean zonal wind averaged over southern subpolar latitudes (55°–65°S) in (a) REF-ORO and (b) MERRA data. (c) Difference between REF-ORO and MERRA. Contour intervals are 10 m s^{-1} in (a) and (b) and 5 m s^{-1} in (c). The thick dashed line denotes the zero-wind contour. Stippling denotes differences statistically insignificant at the 95% confidence level.

Despite the delayed final warming, the cold-pole bias is reduced in REF-ORO by more than a factor of 2 compared to REF. The purple curve in Fig. 3a shows the seasonal climatology of polar cap temperature T at 85 hPa in REF-ORO versus MERRA. The temperature remains within 5 K of the MERRA climatology throughout the year, as shown in Fig. 3b (purple curve). In fact, REF-ORO and MERRA temperatures are statistically indistinguishable from each other at the 95% confidence level in winter (May–July) and during much of the critical ozone hole period (late September–mid-November). During these months, the REF-ORO simulation has cold biases with respect to MERRA that are 2–3 times smaller (less than 5 vs 10–15 K) than the biases in the original simulation, REF (Fig. 3b, black curve).

The improvement in the annual cycle of temperature in REF-ORO produces a corresponding, marked improvement in the simulation of the Antarctic ozone

[1] Note, however, that both REF and REF-ORO share a cold bias with respect to MERRA near the tropopause (~10 km). The source of this bias has not been thoroughly investigated, as it is not directly relevant to the main goals of this study; it may be related to insufficient spatial resolution.

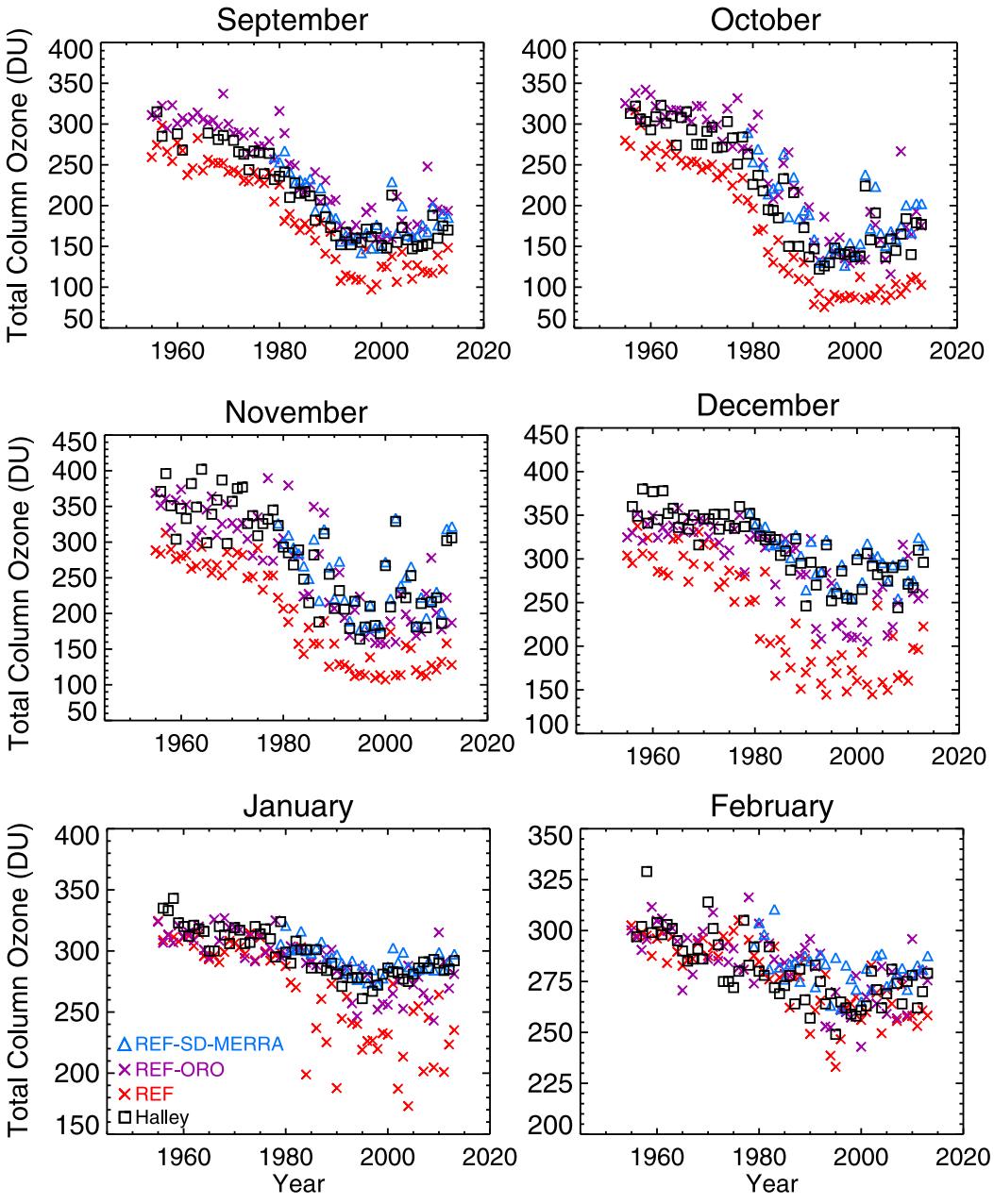

FIG. 5. Monthly mean total ozone column (DU) at Halley Bay (75°S, 26°W) for REF-SD-MERRA (blue triangles); free-running simulations with and without enhanced orographic wave forcing [REF (red crosses) and REF-ORO (purple crosses), respectively]; and ozonesonde data (black squares).

column. Figure 5 shows the evolution of the ozone column at Halley Bay from 1955 to 2013 in REF and REF-ORO compared to the simulation driven by MERRA data, REF-SD-MERRA, and to observations for each month between September and February. The free-running model with enhanced orographic gravity wave forcing (purple crosses) cannot track the year-to-year variability seen in the observations (black squares) like the specified dynamics model (blue triangles) does; however, with one important exception, it reproduces well the monthly behavior of total ozone and, in particular, the development of the ozone hole since the 1970s. The exception is the month of December, when both the observations and REF-SD-MERRA show substantially larger total columns than does REF-ORO. This is a consequence of the delayed breakdown of the

polar vortex discussed above (cf. Fig. 4). By comparison, the results for the original simulation, REF (red symbols), underestimate the ozone column in all months, and especially in December and January due to the very long-delayed and incomplete breakup of the polar vortex in the lower stratosphere in that simulation. Note, finally, that instances of high total ozone column occur more frequently during the ozone hole era in simulation REF-ORO than in the observations. This is consistent with the fact this simulation produces climatological polar cap temperatures that are slightly higher than observed in August–late September (Fig. 3b, purple curve) and suggests that the increase of orographic gravity wave source fluxes in the Southern Hemisphere by a factor of 2 is slightly too large.

c. *The polar mesosphere*

We have shown that enhanced orographic gravity wave fluxes ameliorate the Southern Hemisphere cold-pole bias in WACCM and, in the process, improve the simulation of the Antarctic ozone hole. In doing so, the additional forcing reduces the strength of the Southern Hemisphere polar night jet near 60°S by as much as $25\,\mathrm{m\,s^{-1}}$ in the upper stratosphere (not shown). While the fluxes of other parameterized gravity waves are unaltered, changes in the stratospheric wind systems forced by stronger orographic wave drag could modify the propagation of those gravity waves into the mesosphere and lower thermosphere (MLT) and, therefore, indirectly affect the circulation at higher altitudes (e.g., Holton 1982, 1983).

Of particular importance in simulations of the MLT is the accurate representation of the cold summer mesopause and its warm winter counterpart. These features of the climatology of the MLT are the result of adiabatic cooling in summer (and warming in winter) produced by the gravity wave–driven meridional circulation. In addition to forcing a ''reversed'' meridional temperature gradient in the upper mesosphere, the circulation driven by gravity waves is known to influence many physical and chemical features of this region, including the formation of polar mesospheric clouds (Hervig et al. 2009), the meridional gradients of trace species like water vapor (Garcia et al. 2007), CO and CO_2 (Garcia et al. 2014), seasonal changes in metal layers (Marsh et al. 2013b), and the descent, during winter, of oxides of nitrogen produced by particle precipitation in the auroral regions (Smith et al. 2011).

Although there are no direct measurements of upwelling and downwelling in the polar mesosphere, the temperature and altitude of the polar mesopause in summer and winter are well known, and their accurate simulation is an important measure of the performance of high-top numerical models like WACCM. Marsh et al. (2013a, their Fig. 2) show that the standard version of WACCM reproduces well the altitude and temperature of the summer mesopause as observed by Sounding of the Atmosphere using Broadband Emission Radiometry (SABER), a scanning IR radiometer onboard NASA's *Thermosphere, Ionosphere, Mesosphere Energetics and Dynamics* (*TIMED*) satellite. Figure 6 compares the seasonal cycles of Arctic and Antarctic polar temperature at 0.004 hPa in REF, which does not include enhanced orographic gravity wave forcing, with the seasonal cycle in REF-ORO, which does. In both simulations, the altitude of the summer mesopause is near 0.004 hPa, and its temperature in January drops below 140 K in the southern polar cap. The values in both simulations remain mostly within 5 K of each other throughout much of the year; they are also in good agreement with the SABER observations discussed by Marsh et al. (2013a). SABER temperatures measurements have a standard deviation of 7–10 K at the altitude

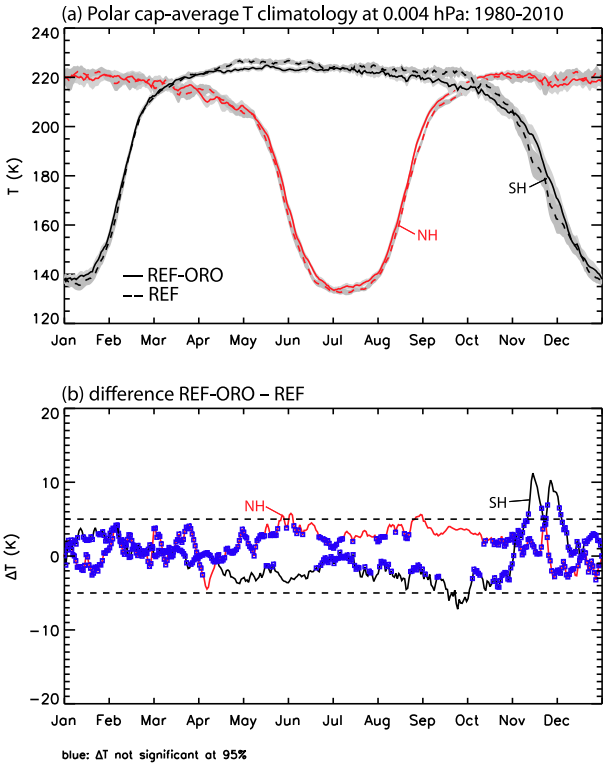

FIG. 6. (a) Seasonal climatology of daily polar cap–average temperature at 0.004 hPa in REF (dashed) and REF-ORO (solid). Gray shading denotes 2σ errors. Results are shown for the Southern Hemisphere (60°–90°S; black) and the Northern Hemisphere (60°–90°N; red). (b) The difference between the two simulations; blue denotes differences insignificant at the 95% level.

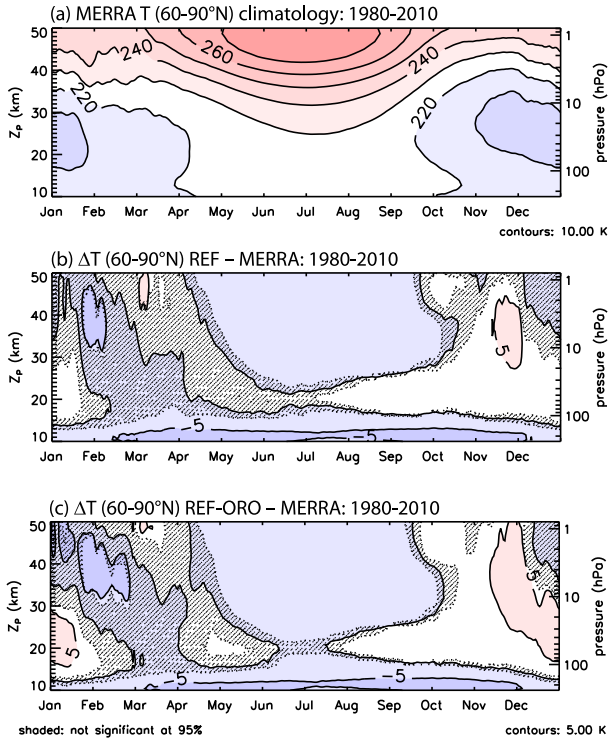

FIG. 7. As in Fig. 2, but for the northern polar cap (60°–90°N).

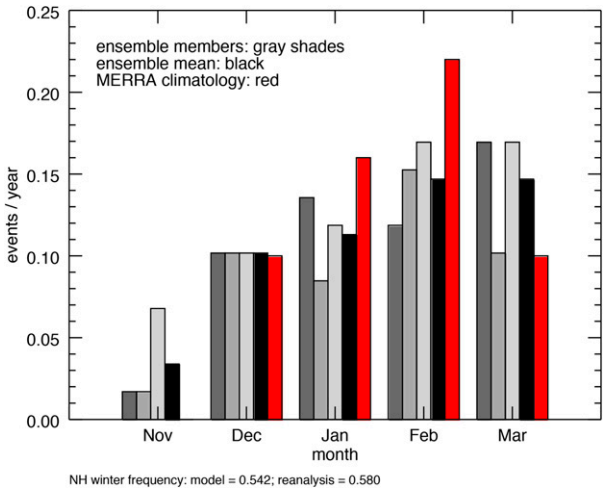

FIG. 8. Monthly frequency distributions of SSW events in a three-member ensemble of REF-ORO simulations and MERRA data. Gray bars denote individual ensemble members and the black bar denotes the ensemble average. Frequencies in the MERRA climatology are denoted by the red bars. See text for details.

of the summer mesopause (Remsberg et al. 2008) such that WACCM simulations, and in particular the results of simulation REF-ORO, agree well with the observations in this region. Thus, the introduction of enhanced orographic fluxes in the WACCM gravity wave parameterization succeeds in ameliorating the cold-pole problem in the Antarctic stratosphere without degrading the simulation of temperature of the polar mesopause in either hemisphere.

d. The Northern Hemisphere stratosphere

The dynamical climatology of the Northern Hemisphere in previous versions of WACCM is in good agreement with observations as regards the seasonal cycle of zonal-mean temperature and zonal wind and the frequency of occurrence of stratospheric sudden warming events (SSW; De la Torre et al. 2012; Marsh et al. 2013a). We examine next to what extent these features are preserved when the orographic gravity wave parameterization is modified in simulation REF-ORO. We emphasize that, while orographic gravity wave fluxes are not altered in the Northern Hemisphere, the removal of the land fraction factor F_L affects both hemispheres, as noted in section 3a and discussed in more detail in section 5.

Figure 7 shows the seasonal cycle of zonal-mean temperature in the Northern Hemisphere derived from MERRA data (Fig. 7a) and the departures from that climatology in the REF and REF-ORO simulations (Figs. 7b and 7c, respectively). The differences from MERRA are not much larger than 5 K in either simulation, and they are statistically insignificant over a substantial part of Northern Hemisphere winter. Small, but statistically significant departures from MERRA are found in summer, when internal variability is very small, and late fall and early winter, when both REF and REF-ORO show small warm biases. A similar comparison for the zonal-mean zonal wind averaged over 55°–65°N (not shown) also reveals small differences from MERRA climatology in both simulations. These comparisons indicate that the modifications to the orographic gravity wave parameterization do not change appreciably the seasonal cycle of zonal-mean temperature and zonal wind in the Northern Hemisphere, which remain close to the MERRA climatology.

Another key indicator of the performance of the model is the ability to reproduce faithfully the observed annual frequency and seasonal distribution of sudden SSW in Northern Hemisphere winter. Figure 8 compares the frequency of major SSW in an ensemble of three REF-ORO simulations against MERRA. We use an ensemble of simulations in this comparison because, as shown by De la Torre et al. (2012), the variability of SSW can be large even among multidecadal model runs. The methodology used to detect SSW is the same as described in the study of De la

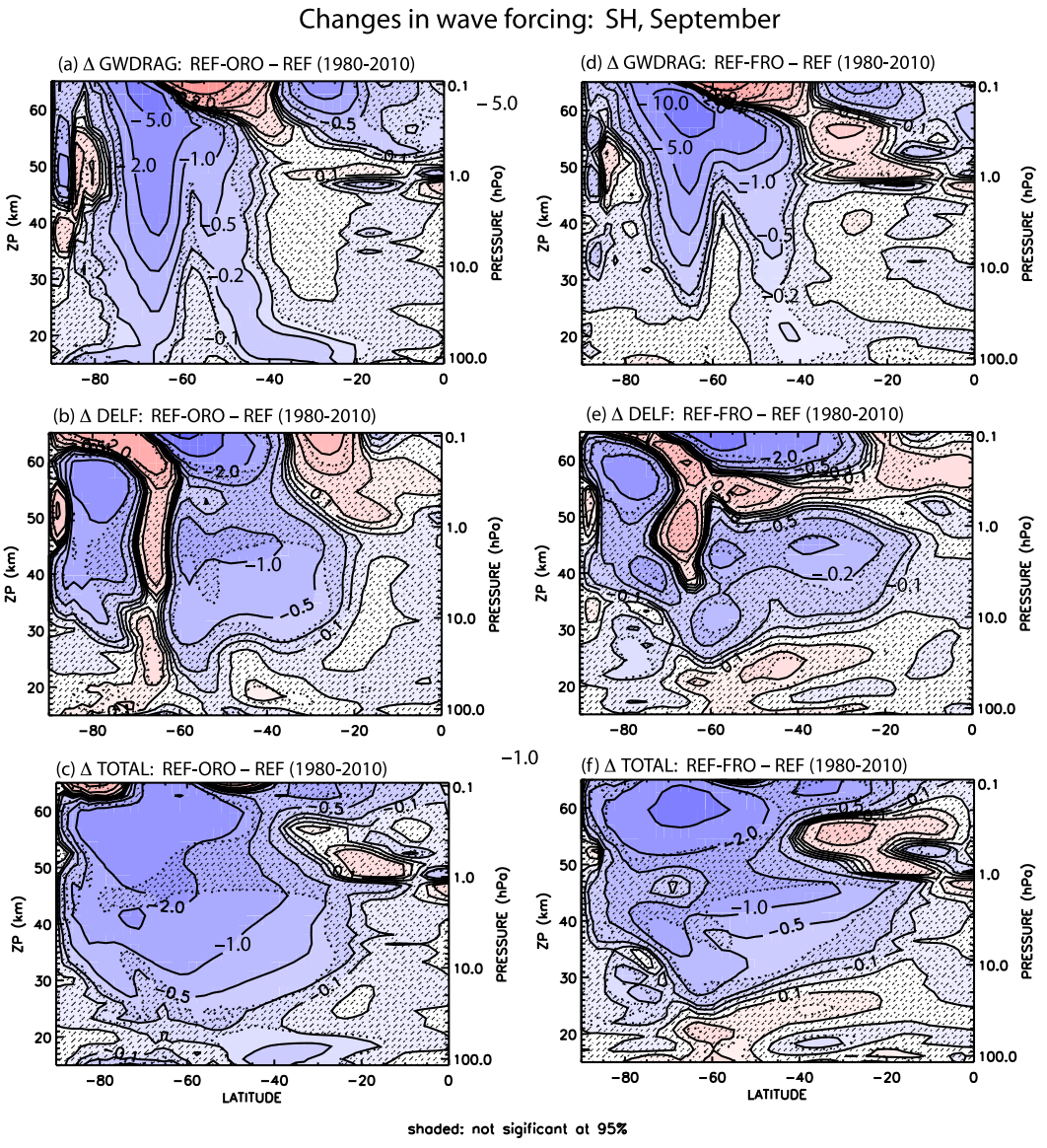

FIG. 9. Change in monthly mean (a) gravity wave drag, (b) Eliassen–Palm flux divergence, and (c) total wave forcing between REF-ORO and REF. (d)–(f) As in (a)–(c), but for REF-FRO and REF. Stippling denotes differences insignificant at the 95% confidence level. Contours are 0, ±0.1, ±0.2, ±0.5, ±1, ±2, ±5, and ±10 m s^{-1} day^{-1}.

Torre et al. (2012) and is applied identically to the REF-ORO simulation and to MERRA data. On an annual basis, major SSW occur with similar frequency in REF-ORO (0.54 yr^{-1}) and MERRA (0.58 yr^{-1}), and the ensemble monthly distribution (black bars in Fig. 8) is also similar to MERRA (red bars). Note, however, that the seasonal distribution of SSW varies among the simulations by as much as 0.07 events per year in some months. This is consistent with the analysis of De la Torre et al. (2012), who found that the 2σ uncertainty of monthly SSW frequencies was ±0.07 events per year in December–March in an earlier version of WACCM. On this basis, the differences in monthly SSW frequency between REF-ORO and MERRA are statistically insignificant.

4. Analysis of polar downwelling in the Southern Hemisphere

Here we examine the changes in the mean meridional downwelling in the Southern Hemisphere stratosphere that result from enhanced orographic gravity wave forcing and attribute them to changes in gravity wave driving. We begin by showing, in Figs. 9a–c, how wave forcing changes

between the standard WACCM simulation, REF, and the simulation with enhanced gravity wave drag, REF-ORO, in the month of September (late winter in the seasonal cycle of the Southern Hemisphere). Figure 9a shows the change in gravity wave drag, which is dominated by orographic drag everywhere below about 55 km. The largest changes in the stratosphere occur around 65°–70°S and are associated with waves excited by the Palmer Peninsula of Antarctica. A smaller maximum, in the latitude range 40°–55°S, is due to orographic forcing over the Southern Andes. Between these maxima lies a region where the change in forcing is small; this is centered at 55°–65°S and corresponds mainly to the Southern Ocean, where orographic gravity wave excitation is weak.

Figures 9b and 9c show the change in EP flux divergence due to resolved waves and the change in total forcing (gravity wave drag plus EP flux divergence), respectively. EP flux divergence also becomes more negative throughout the stratosphere, except in a small range of latitude centered on 65°S, where the change is positive; this region coincides with the location where negative changes in gravity drag are largest. This is evidence of the compensation between different sources of mechanical forcing documented most recently by Sigmond and Shepherd (2014) and references therein. In particular, the latitudinal distribution of total wave forcing (Fig. 9c) is much smoother than the distribution of gravity wave drag or EP flux divergence individually. We show below that this behavior has important implications for attribution of polar downwelling to specific forcing mechanisms.

We consider next how the changes in wave forcing documented above affect downwelling (and hence temperature) at high latitudes of the Southern Hemisphere. Figure 10 shows the vertical component of the transformed Eulerian-mean (TEM) circulation averaged over the Southern Hemisphere polar cap for WACCM simulations with and without increased orographic gravity wave fluxes (REF-ORO and REF, respectively) and their difference. Downwelling is significantly stronger throughout most of the year when the enhanced orographic forcing is included, with the exception of December and January. The latter is simply the result of the very late breakdown of the polar vortex in REF such that strong downwelling extends into Austral summer, whereas in REF-ORO downwelling is much weaker at this time.

The downward control principle (Haynes et al. 1991) can be used to attribute differences in downwelling between REF-ORO and REF to changes in wave forcing. Under downward control, the streamfunction of the steady-state TEM vertical velocity is given by

$$\chi_d^*(\theta, z) = \int_z^\infty \frac{\rho a^2 \cos^2\theta [(\rho a \cos\theta)^{-1} \nabla \cdot \mathbb{F} + \rho^{-1} (\rho \overline{u'w'})_z]}{\overline{m}_\theta} dz', \tag{1}$$

where χ_d^* is the downward control streamfunction; z is log-pressure altitude; $\rho(z)$ is density; θ is latitude; a is the radius of Earth; $\nabla \cdot \mathbb{F}$ is the divergence of the EP flux due to resolved waves; $(\rho\overline{u'w'})_z$ is the divergence of the eddy momentum flux due to (parameterized) gravity waves; and $\overline{m}_\theta$ is the meridional gradient of zonal-mean angular momentum. The TEM vertical velocity can then be obtained from the streamfunction according to

$$w_d^*(\theta, z) = \frac{1}{\rho(z)\cos\theta} \frac{1}{a} \frac{\partial \chi_d^*}{\partial \theta}. \tag{2}$$

With (1) and (2), one can formally attribute χ_d^* and w_d^* to the individual contributions of large-scale waves, $\nabla \cdot \mathbb{F}$, and gravity wave drag, $(\rho\overline{u'w'})_z$, since these terms are linearly additive in (1).

When the results of our simulations are analyzed in this way, we find that the acceleration of the TEM circulation in REF-ORO relative to REF is not due simply to the difference in gravity wave drag between the two simulations. Instead, there is a large degree of compensation between $\nabla \cdot \mathbb{F}$ and $(\rho\overline{u'w'})_z$. For example, Fig. 11 shows χ_d^* at 72 hPa (~19 km) in September in REF and REF-ORO, and the difference between the two simulations. (We show 72 hPa because this level lies immediately above the core of the ozone hole, but similar results are obtained at other levels). Austral late winter and spring is the time of the year when the stronger downwelling over the southern polar cap in REF-ORO (cf. Fig. 10) leads to warmer temperatures and a much-improved simulation of the Antarctic ozone column (Fig. 5). In Fig. 11, the black curves denote the total streamfunction, and the blue and red curves are the contributions due to $\nabla \cdot \mathbb{F}$ and $(\rho\overline{u'w'})_z$, respectively.[2] In simulation REF (Fig. 11a), where gravity wave forcing in the lower stratosphere is weak on the pressure level shown, there is little indication of compensation between the contributions of EP flux divergence and gravity wave forcing. On the other

[2] Note that the total streamfunction is not in general equal to the sum of the contributions of EP flux divergence and gravity wave drag because, on monthly time scales, the change in the zonal-mean zonal wind is not negligible, and downward control does not apply exactly.

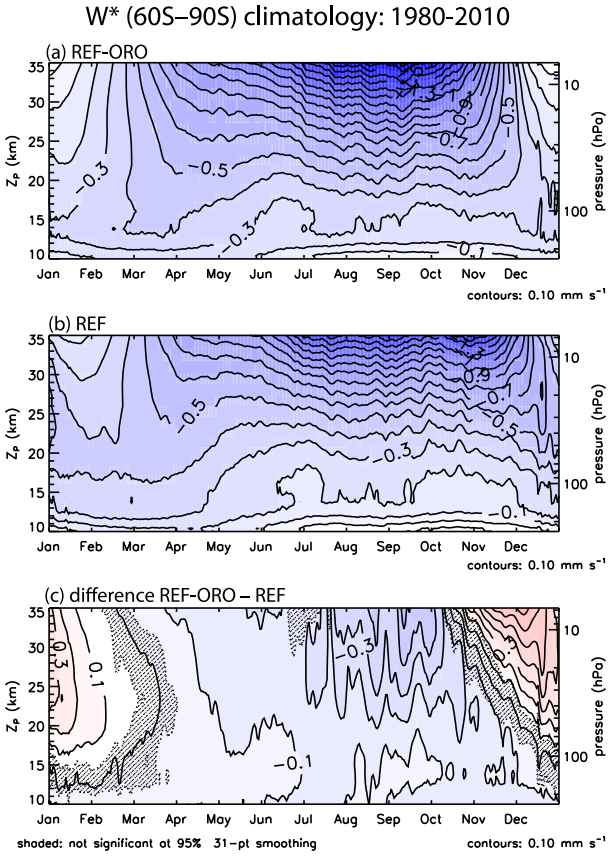

FIG. 10. Climatological seasonal cycle (1980–2010) of daily TEM vertical velocity (mm s^{-1}) averaged over the southern polar cap (60°–90°S) in (a) REF-ORO and (b) REF. (c) Difference between (a) and (b). Stippling denotes differences statistically insignificant at the 95% level. Contours are 0.1 mm s^{-1} in all panels. Results have been smoothed with a 31-day running mean to improve readability.

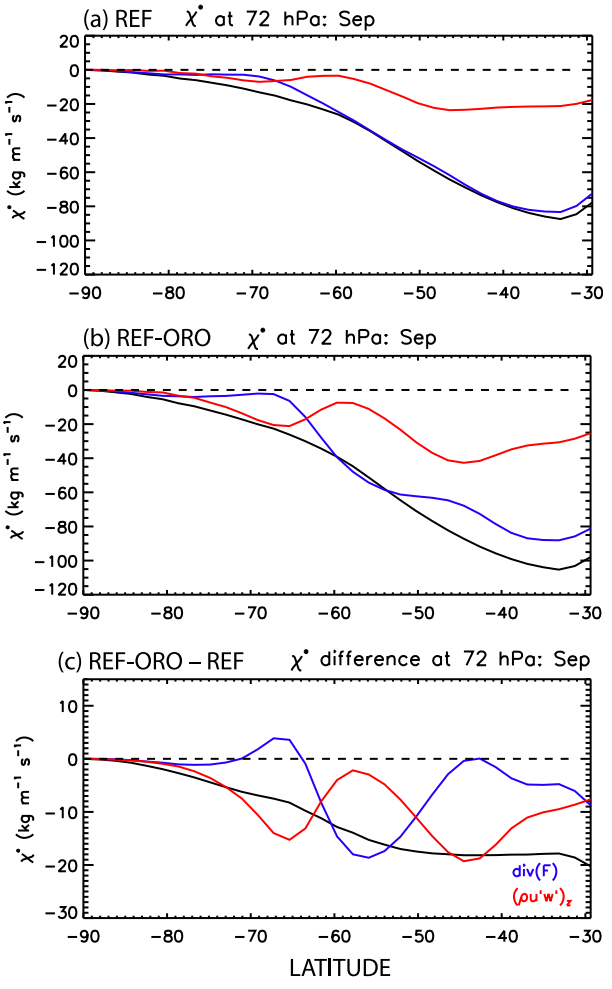

FIG. 11. The mean meridional downward control streamfunction for (a) REF, (b) REF-ORO, and (c) the difference of REF-ORO minus REF. The black lines denote the total streamfunction. The blue and red lines denote the contributions due to EP flux divergence and gravity wave drag, respectively. See text for details.

hand, in REF-ORO (Fig. 11b), where forcing by gravity waves becomes substantial throughout the stratosphere, the EP flux divergence changes such that it compensates the effects of the enhanced gravity wave forcing. This can be seen most clearly in Fig. 11c, which shows the difference in the streamfunction between REF and REF-ORO.

These results agree well with the study of Cohen et al. (2013), who used a mechanistic, primitive equation model to study the compensation between EP flux divergence and gravity wave forcing. Cohen et al. (2013) argued that compensation occurs because enhanced gravity wave driving produces an unstable zonal-mean state, which is stabilized by the response of resolved EP flux divergence, and that compensation is most likely to occur when gravity wave drag is strong and may be absent when gravity wave drag is weak. The strong cancellation of the contributions to χ_d^* by gravity wave drag and EP flux divergence seen in our REF-ORO simulation, and in the difference between REF-ORO and REF, is consistent with Cohen et al.'s (2013) findings. The role of instability in the compensation phenomenon has been questioned by Sigmond and Shepherd (2014), who found no clear evidence of instability in model calculations that otherwise exhibited compensation behavior. Ming et al. (2016) have addressed the question via scale analysis of the zonal-mean momentum equation and concluded that the response to a latitudinally "narrow" change in mechanical forcing (which, in the present context, may be envisaged as a change in gravity wave drag) will tend to be compensated by changes of the opposite sign in other wave forcing (such as EP flux divergence). Nevertheless, the analysis of Ming et al.

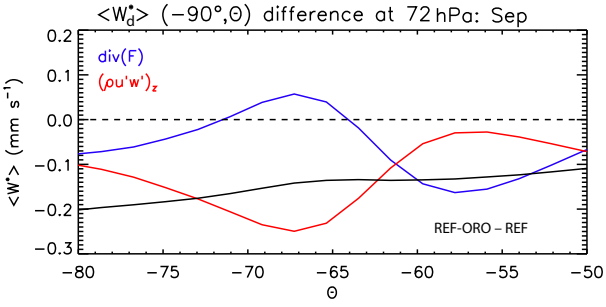

FIG. 12. Difference in polar cap–average "downward control" vertical velocity $\langle w_d^*(z)\rangle$ (black curve) between simulations REF-ORO and REF as a function of the latitude θ used to define the equatorward edge of the polar cap. The blue and red curves denote the attribution of $\langle w_d^*(z)\rangle$ to EP flux divergence and gravity wave drag, respectively.

(2016) does not constrain the mechanism whereby EP flux divergence changes to compensate for a change in gravity wave drag. Indeed, Cohen et al. (2014) show that compensation can occur via instability of the background flow, and also by the effect of gravity wave drag on the background potential vorticity gradient, which conditions the propagation and dissipation of Rossby waves; see, in particular, Cohen et al.'s (2014) Fig. 8 and related discussion.

Cohen et al. (2013) concluded that compensation between resolved and parameterized wave driving implies that separating wave forcing via downward control can be misleading. In the present context, the problem can be appreciated from Fig. 11. There we see that, while the contribution of gravity wave forcing to χ_d^* has increased roughly twofold in REF-ORO relative to REF, the EP flux divergence has adjusted to compensate a substantial fraction of this forcing locally such that the total change in χ_d^* (Fig. 11c, black curve) is much smoother in latitude than the change attributable to $\nabla\cdot\mathbb{F}$ or $(\rho\overline{u'w'})_z$ alone (blue and red curves, respectively). In this example, compensation leads to peculiar results if one attempts to attribute polar cap–average downwelling to resolved versus parameterized waves. From (2), the (cosine weighted) average downwelling between some latitude θ used to define the edge of the polar cap and the pole is

$$\langle w_d^*(z)\rangle = \frac{1}{\rho(z)}\int_{-\pi/2}^{\theta}\frac{1}{a}\frac{\partial\chi_d^*}{\partial\theta}d\theta' \Big/ \int_{-\pi/2}^{\theta}\cos\theta' d\theta' = \frac{\chi_d^*(\theta,z)}{\rho(z)a(\sin\theta+1)}, \tag{3}$$

which depends only on χ_d^* at the edge of the polar cap θ because the streamfunction vanishes at the pole.

Applying (3) to the streamfunction difference shown in Fig. 11c produces the result illustrated in Fig. 12, which shows the polar cap–average vertical velocity between the South Pole and the latitude indicated in the abscissa. If the average is taken from the pole to any latitude between 65° and 75°S, the change in $\langle w_d^*(z)\rangle$ would be attributed mainly to gravity wave drag (red curve), but, if the average is taken from the pole to latitudes between 55° and 60°S, the change would be attributed mainly to EP flux divergence (blue curve). In particular, downward control would ascribe most of the difference in $\langle w_d^*(z)\rangle$ shown in Fig. 10 (60°–90°S average) to changes in EP flux divergence. However, had we defined the polar cap as latitudes 65°–90°S, the difference in $\langle w_d^*(z)\rangle$ would be attributed to changes in gravity wave drag. Thus, a naïve interpretation of (3) leads to completely different attribution of changes in polar cap downwelling when the edge of the polar cap changes by only a few degrees of latitude. Of course, we know—by construction—that the change in downwelling in the Southern Hemisphere is due to our modification of the orographic gravity wave parameterization, which has increased the upward flux of these waves at their source. However, this change does not happen simply through a linear response to orographic gravity wave drag; instead, the change in downwelling is established after substantial compensation between gravity wave drag and EP flux divergence.

The compensation phenomenon implies that the enhancement of polar downwelling by stronger gravity wave drag is not very sensitive to the latitude where the enhanced wave drag occurs. Several recent papers (e.g., Sato et al. 2012; Alexander and Grimsdell 2013; Hindley et al. 2015) have addressed the question of insufficient wave drag over the Southern Ocean, around 60°S, identified by McLandress et al. (2012) in the Canadian Middle Atmosphere Model (CMAM). McLandress et al. (2012) showed that introducing an ad hoc source of additional orographic gravity waves centered on 60°S reduced substantially the Southern Hemisphere cold-pole bias in CMAM. However, in the present study we have merely increased the existing source fluxes of orographic gravity wave drag in WACCM without attempting to address specifically the forcing "gap" around 60°S, where the orographic gravity wave parameterization produces weak wave fluxes. Indeed, this region of weak forcing remains (cf. Figs. 9a and 11b) even when forcing at other latitudes increases. Nevertheless, the REF-ORO simulation produces stronger downwelling throughout the polar cap, as implied by the smooth behavior of the total streamfunction difference shown in Fig. 11c and by the

distribution of the change in total forcing in Fig. 9c. The gap in gravity wave forcing near 60°S is filled by a compensating increase in resolved EP flux divergence.

5. Discussion

Our finding that changes to orographic wave fluxes can ameliorate the Antarctic cold-pole bias in WACCM while preserving desirable aspects of the model's climatology elsewhere may be considered circumstantial evidence for the importance of orographic wave forcing in the Southern Hemisphere. We might ask, however, whether the results imply that the cold-pole bias is uniquely addressed through modification of the orographic component of the gravity wave parameterization or whether the deficit of gravity wave forcing in the Southern Hemisphere could be remedied by other plausible changes to the gravity wave parameterization in WACCM.

To explore this question, we experimented with a modification to the parameterization of gravity waves excited by fronts. The standard version of this parameterization, described by Richter et al. (2010), evaluates a frontogenesis function and launches a spectrum of gravity waves whenever the result exceeds a certain threshold. The magnitude of the source flux is a tunable parameter, which is assigned a fixed value [currently 1.5 mPa at 500 hPa; Richter et al. (2010)]. However, observations of gravity wave fluxes over the Southern Ocean, presumably associated with the passage of frontal zones, exhibit very large variability such that their magnitude is best described by a lognormal distribution (e.g., Hertzog et al. 2012; Jewtoukoff et al. 2015; Alexander et al. 2016). Following De la Cámara et al. (2016), we account for this behavior by selecting the source flux at random from a lognormal distribution that resembles observations and retains a mean value of 1.5 mPa. We refer to the simulation that incorporates this approach as REF-FRO and emphasize that no changes to the orographic wave sources are included therein.

Figures 9c–e shows the change in wave forcing between simulation REF-FRO and the standard WACCM simulation, REF. Changes to gravity wave drag are now due mainly to waves excited by fronts, which are largest in the lower mesosphere, above about 50 km (Fig. 13d). In addition, the resulting weakening of the polar jet allows orographic gravity waves to saturate and "break" at lower levels and accounts for the larger gravity wave drag between about 30 and 50 km. In the lower stratosphere, below 30 km, the difference in forcing is actually dominated by changes in EP flux divergence (cf. Figs. 9e and 9f). As in REF-ORO, the run with enhanced frontal gravity waves exhibits a high degree of compensation such that the total change in forcing (Fig. 9f) is much smoother in latitude than the changes due to gravity wave drag and EP flux divergence individually (Figs. 9d,e).

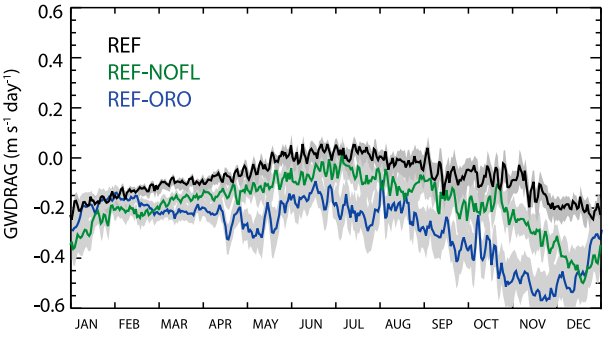

FIG. 13. Seasonal cycle of daily orographic gravity wave drag ($m\,s^{-1}\,day^{-1}$) at 30 hPa, averaged over 50°–70°S in REF, REF-ORO, and REF-NOFL. Shading denotes 2σ errors. See text for details.

The green curves in Fig. 3 show the climatology of polar cap temperature (60°–90°S) in REF-FRO at 85 hPa (Fig. 3a) and its departure from MERRA (Fig. 3b). The cold-pole bias in REF-FRO is substantially reduced with respect to the standard simulation REF, although it remains larger than in REF-ORO, in particular during the Antarctic ozone hole season, September–November (cf. green and purple curves in Fig. 3b). This follows from the fact that the increase in polar cap downwelling in the lower stratosphere is weaker in REF-FRO than in REF-ORO (not shown), as expected from the change in wave forcing (cf. Figs. 9c and 9f). Since no systematic attempt was made to optimize the REF-FRO simulation, it might be possible to improve on these results by varying the parameters of the lognormal distribution that defines the source amplitude of gravity waves excited by fronts such that large-amplitude events occur more frequently. Stronger downwelling and a warmer polar cap might also be achieved by increasing the mean value of the distribution; however, based upon prior experience with WACCM, this will likely degrade the climatology of the mesosphere, which is strongly controlled by forcing due to gravity waves generated by fronts.

Perhaps the most important inference to be drawn from these results is that a high-top model with coupled chemistry introduces very strong constraints on the tuning of gravity wave parameterizations. While there are numerous ways to ameliorate the cold-pole bias in the Southern Hemisphere in WACCM, only a small subset of those does not degrade the simulation elsewhere. Thus, the success of changes to the orographic gravity wave parameterization documented here provides

strong circumstantial support for the crucial role of orographic gravity waves, especially in the Southern Hemisphere.

Given the importance of orographic gravity wave forcing in WACCM, we have also explored the relative importance of the two changes introduced in the parameterization: the elimination of the land fraction factor F_L and the increase, by a factor of 2, of the orographic source flux in the Southern Hemisphere. To illustrate the relative importance of these changes, Fig. 13 compares the seasonal cycle of gravity wave drag at 30 hPa (~25 km) averaged over 50°–70°S in the standard model REF (black curve), REF-ORO (purple curve), and a version of the model where the only change is the removal of F_L (REF-NOFL; green curve). Removing F_L leads to a nonnegligible increase in wave drag, which is statistically significant with respect to REF much of the year. Nevertheless, the twofold increase in source fluxes in REF-ORO produces an even larger additional increase in the overall drag and is necessary to eliminate the cold-pole bias. We examined the evolution of temperature in the southern polar cap at 85 hPa in REF-NOFL (not shown) and found that the removal of F_L accounts for at most 25%–40% of the improvement in the climatology of T (85 hPa) illustrated in Fig. 3, depending on the time of the year.[3] These findings are typical of the entire stratosphere, not just the pressure level shown in Fig. 13.

6. Summary and conclusions

We have shown that modifying the orographic gravity wave parameterization used in WACCM such that the source fluxes are enhanced preferentially in the Southern Hemisphere results in a much-improved simulation of the dynamical and chemical structure of the Antarctic polar vortex. The changes in the gravity wave parameterization address the model's cold-pole bias in the Antarctic stratosphere, which has been present in all earlier versions of WACCM. The cold bias has especially undesirable consequences for the simulation of the Antarctic ozone hole. The enhanced orographic wave forcing warms the Antarctic lower stratosphere, producing temperatures that are very close to the MERRA climatology over much of the year (Fig. 3) and improving markedly the simulation of ozone (Fig. 5).

We have also examined other aspects of the simulation with enhanced orographic forcing to ascertain that addressing the Antarctic cold-pole bias is not achieved at the expense of degrading the model performance in other regions or seasons. We have shown that the zonal-mean zonal wind climatology in the Southern Hemisphere is also improved in the new simulation and that other features, such as the location and temperature of the summer mesopause (Fig. 6) and the climatology of zonal-mean temperature and zonal wind in the Northern Hemisphere, remain close to observations. The climatology of major SSW in northern winter is also realistic in the simulation with enhanced orographic gravity wave forcing (Fig. 8).

We emphasize that, in the simulation discussed here, the orographic source fluxes in the Southern Hemisphere were increased, somewhat arbitrarily, by a factor of 2. While the increase is motivated by the likelihood that fluxes in the Southern Hemisphere are underestimated in the current parameterization, a more precise evaluation will require reformulation of the orographic gravity wave parameterization to take into account explicitly the orientation of the prevailing local flow with respect to topography (e.g., Scinocca and McFarlane 2000). Therefore, the results presented here might be viewed as a sensitivity test of the impact of enhanced gravity wave driving, by a specific source of gravity waves, on the circulation and temperature of the Antarctic stratosphere.

In addition, the question of what accounts for the "missing" gravity wave forcing in the standard simulation (REF) may have more than one plausible answer, and an improved representation of gravity wave forcing might include modifications to more than one component of the gravity wave parameterization, as discussed in section 5. The downward control analysis presented in section 4 suggests that it is difficult to establish the "most realistic" distribution of gravity wave sources based on a single criterion, such as improvement of the cold-pole bias. The cold bias in WACCM is mostly eliminated through stronger polar downwelling driven by increasing orographic gravity wave drag; however, as demonstrated in section 4, this does not require increasing gravity wave fluxes over the latitude band spanned by the Southern Ocean, where orographic forcing is weak. Instead, we find that the EP flux divergence due to resolved waves adjusts to compensate the new pattern of gravity wave forcing such that there is a latitudinally smooth increase in forcing throughout the stratosphere (Fig. 9). This conclusion is in line with the findings of Cohen et al. (2013) and Sigmond and Shepherd (2014). Nevertheless, an accurate apportionment of gravity wave forcing should still be important for simulating realistically the global climate and, in

[3] In the Northern Hemisphere, F_L has no significant impact on the climatology of orographic gravity wave drag or polar cap temperature (not shown), consistent with our expectation that the removal of F_L is most important in the Southern Hemisphere.

particular, its response to natural and anthropogenic perturbations. To this end, careful examination of observational results that document the geographical distribution, seasonal variation, amplitude, and intermittency of gravity wave fluxes (e.g., Ern and Preusse 2012; Geller et al. 2013; Alexander 2015; Smith et al. 2016), together with sophisticated evaluation of downward control diagnostics, will be required.

Acknowledgments. We thank Drs. J. Richter and J.-F. Lamarque for their comments on the original version of this study. We also thank Drs. Ed Gerber and Peter Haynes and an anonymous reviewer for their reviews, which have resulted in a much improved paper, and Dr. Jonathan Shanklin, of the British Antarctic Survey, for making available the Halley total column ozone data. R. Garcia was supported in part by NASA Grant X09AJ83G. WACCM is a component of the Community Earth System Model (CESM), which is supported by the NSF and the Office of Science of the U.S. Department of Energy. Computing resources were provided by NCAR's Climate Simulation Laboratory, sponsored by the NSF and other agencies. This research was enabled by the computational and storage resources of NCAR's Computational and Information Systems Laboratory (CISL).

REFERENCES

Alexander, M. J., 2015: Global and seasonal variations in three-dimensional gravity wave momentum flux from satellite limb-sounding temperatures. *Geophys. Res. Lett.*, **42**, 6860–6867, doi:10.1002/2015GL065234.

——, and A. W. Grimsdell, 2013: Seasonal cycle of orographic gravity wave occurrence above small islands in the Southern Hemisphere: Implications for effects on the general circulation. *J. Geophys. Res. Atmos.*, **118**, 11 589–11 599, doi:10.1002/2013JD020526.

Alexander, S. P., K. Sato, S. Watanabe, Y. Kawatani, and D. J. Murphy, 2016: Southern Hemisphere extratropical gravity wave sources and intermittency revealed by a middle-atmosphere general circulation model. *J. Atmos. Sci.*, **73**, 1335–1349, doi:10.1175/JAS-D-15-0149.1.

Beres, J. H., R. R. Garcia, B. A. Boville, and F. Sassi, 2005: Implementation of a gravity wave source spectrum parameterization dependent on the properties of convection in the Whole Atmosphere Community Climate Model (WACCM). *J. Geophys. Res.*, **110**, D10108, doi:10.1029/2004JD005504.

Cohen, N. Y., E. P. Gerber, and O. Bühler, 2013: Compensation between resolved and unresolved wave driving in the stratosphere: Implications for downward control. *J. Atmos. Sci.*, **70**, 3780–3798, doi:10.1175/JAS-D-12-0346.1.

——, ——, and ——, 2014: What drives the Brewer–Dobson circulation? *J. Atmos. Sci.*, **71**, 3837–3855, doi:10.1175/JAS-D-14-0021.1.

De la Cámara, A., F. Lott, V. Jewtoukoff, R. Plougonven, and A. Hertzog, 2016: On the gravity wave forcing during the southern stratospheric final warming in LMDZ. *J. Atmos. Sci.*, **73**, 3213–3226, doi:10.1175/JAS-D-15-0377.1.

De la Torre, L., R. R. Garcia, D. Barriopedro, and A. Chandran, 2012: Climatology and characteristics of stratospheric sudden warmings in the Whole Atmosphere Community Climate Model. *J. Geophys. Res.*, **117**, D04110, doi:10.1029/2011JD016840.

Ern, M., and P. Preusse, 2012: Gravity wave momentum flux spectra observed from satellite in the summertime subtropics: Implications for global modeling. *Geophys. Res. Lett.*, **39**, L15810, doi:10.1029/2012GL052659.

Garcia, R. R., D. R. Marsh, D. E. Kinnison, B. A. Boville, and F. Sassi, 2007: Simulation of secular trends in the middle atmosphere, 1950–2003. *J. Geophys. Res.*, **112**, D09301, doi:10.1029/2006JD007485.

——, M. López-Puertas, B. Funke, D. R. Marsh, D. E. Kinnison, A. K. Smith, and F. González-Galindo, 2014: On the distribution of CO_2 and CO in the mesosphere and lower thermosphere. *J. Geophys. Res. Atmos.*, **119**, 5700–5718, doi:10.1002/2013JD021208.

Geller, M., and Coauthors, 2013: A comparison between gravity wave momentum fluxes in observations and climate models. *J. Climate*, **26**, 6383–6405, doi:10.1175/JCLI-D-12-00545.1.

Haynes, P. H., C. J. Marks, M. E. McIntyre, T. G. Shepherd, and K. P. Shine, 1991: On the "downward control" of extratropical diabatic circulations by eddy-induced mean zonal forces. *J. Atmos. Sci.*, **48**, 651–678, doi:10.1175/1520-0469(1991)048<0651:OTCOED>2.0.CO;2.

Hendricks, E. A., J. D. Doyle, S. D. Eckermann, Q. Jiang, and P. A. Reinecke, 2014: What is the source of the stratospheric gravity wave belt in austral winter? *J. Atmos. Sci.*, **71**, 1583–1592, doi:10.1175/JAS-D-13-0332.1.

Hertzog, A., M. J. Alexander, and R. Plougonven, 2012: On the intermittency of gravity wave momentum flux in the stratosphere. *J. Atmos. Sci.*, **69**, 3433–3448, doi:10.1175/JAS-D-12-09.1.

Hervig, M. E., M. H. Stevens, L. L. Gordley, L. E. Deaver, J. M. Russell III, and S. M. Bailey, 2009: Relationships between polar mesospheric clouds, temperature, and water vapor from Solar Occultation for Ice Experiment (SOFIE) observations. *J. Geophys. Res.*, **114**, D20203, doi:10.1029/2009JD012302.

Hindley, N. P., C. J. Wright, N. D. Smith, and N. J. Mitchell, 2015: The southern stratospheric gravity wave hot spot: Individual waves and their momentum fluxes measured by COSMIC GPS-RO. *Atmos. Chem. Phys.*, **15**, 7797–7818, doi:10.5194/acp-15-7797-2015.

Holton, J. R., 1982: The role of gravity wave momentum drag and diffusion in the momentum budget of the mesosphere. *J. Atmos. Sci.*, **39**, 791–799, doi:10.1175/1520-0469(1982)039<0791:TROGWI>2.0.CO;2.

——, 1983: The influence of gravity wave breaking on the general circulation of the middle atmosphere. *J. Atmos. Sci.*, **40**, 2497–2507, doi:10.1175/1520-0469(1983)040<2497:TIOGWB>2.0.CO;2.

Jewtoukoff, V., A. Hertzog, R. Plougonven, A. de la Cámara, and F. Lott, 2015: Comparison of gravity waves in the Southern Hemisphere derived from balloon observations and the ECMWF analyses. *J. Atmos. Sci.*, **72**, 3449–2468, doi:10.1175/JAS-D-14-0324.1.

Kinnison, D. E., and Coauthors, 2007: Sensitivity of chemical tracers to meteorological parameters in the MOZART-3 chemical transport model. *J. Geophys. Res.*, **112**, D20302, doi:10.1029/2006JD007879.

Kunz, A., L. L. Pan, P. Konopka, D. E. Kinnison, and S. Tilmes, 2011: Chemical and dynamical discontinuity at the extratropical

tropopause based on START08 and WACCM analyses. *J. Geophys. Res.*, **116**, D24302, doi:10.1029/2011JD016686.

Lamarque, J. F., and Coauthors, 2012: CAM-Chem: Description and evaluation of interactive atmospheric chemistry in the Community Earth System Model. *Geosci. Model Dev.*, **5**, 369–411, doi:10.5194/gmd-5-369-2012.

Marsh, D. R., 2011: Chemical–dynamical coupling in the mesosphere and lower thermosphere. *Aeronomy of the Earth's Atmosphere and Ionosphere*, M. A. Abdu, D. Pancheva, and A. Bhattacharyya, Eds., IAGA Special Sopron Book Series, Vol. 2, Springer, 3–17, doi:10.1007/978-94-007-0326-1_1.

——, M. E. Mills, D. E. Kinnison, J.-F. Lamarque, N. Calvo, and L. M. Polvani, 2013a: Climate change from 1850 to 2005 simulated in CESM1 (WACCM). *J. Climate*, **26**, 7372–7391, doi:10.1175/JCLI-D-12-00558.1.

——, D. Janches, W. Feng, and J. M. C. Plane, 2013b: A global model of meteoric sodium. *J. Geophys. Res. Atmos.*, **118**, 11 442–11 452, doi:10.1002/jgrd.50870.

McFarlane, N. A., 1987: The effect of orographically excited wave drag on the general circulation of the lower stratosphere and troposphere. *J. Atmos. Sci.*, **44**, 1775–1800, doi:10.1175/1520-0469(1987)044<1775:TEOOEG>2.0.CO;2.

McLandress, C., T. G. Shepherd, S. Polavaparu, and S. R. Beagley, 2012: Is missing orographic gravity wave drag near 60°S the cause of the stratospheric zonal wind biases in chemistry–climate models? *J. Atmos. Sci.*, **69**, 802–818, doi:10.1175/JAS-D-11-0159.1.

Ming, A., P. Hitchcock, and P. Haynes, 2016: The response of the lower stratosphere to zonally symmetric thermal and mechanical forcing. *J. Atmos. Sci.*, **73**, 1903–1922, doi:10.1175/JAS-D-15-0294.1.

Neale, R., J. Richter, S. Park, P. Lauritzen, S. Vavrus, P. Rasch, and M. Zhang, 2013: The mean climate of the Community Atmosphere Model (CAM4) in forced SST and fully coupled experiments. *J. Climate*, **26**, 5150–5168, doi:10.1175/JCLI-D-12-00236.1.

Rayner, N. A., D. E. Parker, E. B. Horton, C. K. Folland, L. V. Alexander, D. P. Rowell, E. C. Kent, and A. Kaplan, 2003: Global analyses of sea surface temperatures, sea ice, and night marine air temperature since the late nineteenth century. *J. Geophys. Res.*, **108**, 4407, doi:10.1029/2002JD002670.

Remsberg, E. E., and Coauthors, 2008: Assessment of the quality of the version 1.07 temperature-versus-pressure profiles of the middle atmosphere from TIMED/SABER. *J. Geophys. Res.*, **113**, D17101, doi:10.1029/2008JD010013.

Richter, J. H., F. Sassi, and R. R. Garcia, 2010: Towards a physically based gravity wave source parameterization in a general circulation model. *J. Atmos. Sci.*, **67**, 136–156, doi:10.1175/2009JAS3112.1.

Rienecker, M. M., and Coauthors, 2011: MERRA: NASA's Modern-Era Retrospective Analysis for Research and Applications. *J. Climate*, **24**, 3624–3648, doi:10.1175/JCLI-D-11-00015.1.

Sato, K., S. Tateno, S. Watanabe, and Y. Kawatani, 2012: Gravity wave characteristics in the Southern Hemisphere revealed by a high-resolution middle-atmosphere general circulation model. *J. Atmos. Sci.*, **69**, 1378–1396, doi:10.1175/JAS-D-11-0101.1.

Scinocca, J. F., and N. A. McFarlane, 2000: The parametrization of drag induced by stratified flow over anisotropic orography. *Quart. J. Roy. Meteor. Soc*, **126**, 2353–2393, doi:10.1002/qj.49712656802.

Shibuya, R., K. Sato, Y. Tomikawa, M. Tsutsumi, and T. Sato, 2015: A study of multiple tropopause structures caused by inertia–gravity waves in the Antarctic. *J. Atmos. Sci.*, **72**, 2109–2130, doi:10.1175/JAS-D-14-0228.1.

Sigmond, M., and T. G. Shepherd, 2014: Compensation between resolved wave driving and parameterized orographic gravity wave driving of the Brewer–Dobson circulation and its response to climate change. *J. Climate*, **27**, 5601–5610, doi:10.1175/JCLI-D-13-00644.1.

Smith, A. K., R. R. Garcia, D. R. Marsh, and J. H. Richter, 2011: WACCM simulations of the mean meridional circulation and trace species transport in the winter mesosphere. *J. Geophys. Res.*, **116**, D20115, doi:10.1029/2011JD016083.

Smith, R., and Coauthors, 2016: Stratospheric gravity wave fluxes and scales during DEEPWAVE. *J. Atmos. Sci.*, **73**, 2851–2869, doi:10.1175/JAS-D-15-0324.1.

Solomon, S., D. Kinnison, J. Bandoro, and R. Garcia, 2015: Simulation of polar ozone depletion: An update. *J. Geophys. Res. Space Phys.*, **120**, 2183–2193, doi:10.1002/2014JA020886.

Wegner, T., D. E. Kinnison, R. R. Garcia, and S. Solomon, 2013: Simulation of polar stratospheric clouds in the specified dynamics version of the whole atmosphere community climate model. *J. Geophys. Res. Atmos.*, **118**, 4991–5002, doi:10.1002/jgrd.50415.

Wright, C. J., S. M. Osprey, and J. C. Gille, 2013: Global observations of gravity wave intermittency and its impact on the observed momentum flux morphology. *J. Geophys. Res. Atmos.*, **118**, 10 980–10 993, doi:10.1002/jgrd.50869.